Published in final edited form as:
J Alzheimers Dis. 2014 ; 39(1): 71–78. doi:10.3233/JAD-131526.

Corpus Callosum Shape and Size Changes in Early Alzheimer's Disease: A Longitudinal MRI Study Using the OASIS Brain Database

Alvin H. Bachman[a], **Sang Han Lee**[a], **John J. Sidtis**[a,b], and **Babak A. Ardekani**[a,b,*]

[a]The Nathan S. Kline Institute for Psychiatric Research, Orangeburg, NY, USA

[b]Department of Psychiatry, New York University School of Medicine, New York, NY, USA

Abstract

Background—Alzheimer's disease (AD) has been shown to be associated with shrinkage of the corpus callosum mid-sagittal cross-sectional area (CCA).

Objective—To study temporal rates of corpus callosum atrophy not previously reported for early AD.

Methods—We used longitudinal MRI scans to study the rates of change of CCA and circularity (CIR), a measure of its shape, in normal controls (NC, $n = 75$), patients with very mild AD (AD-VM, $n = 51$), and mild AD (AD-M, $n = 21$).

Results—There were significant reduction rates in CCA and CIR in all three groups. While CCA reduction rates were not statistically different between groups, the CIR declined faster in AD-VM ($p < 0.03$) and AD-M ($p < 0.0001$) relative to NC, and in AD-M relative to AD-VM ($p < 0.0004$).

Conclusion—CIR declines at an accelerated rate with AD severity. Its rate of change is more closely associated with AD progression than CCA or any of its sub-regions. CIR may be a useful group biomarker for objective assessment of treatments that aim to slow AD progression.

Keywords

Alzheimer's disease; brain; circularity; corpus callosum; magnetic resonance imaging; shape analysis

INTRODUCTION

The corpus callosum (CC) is the largest fiber tract in the nervous system, connecting homotopic cortical regions in the two cerebral hemispheres. Functionally, it provides interhemispheric transfer of sensory, motor, and cognitive information [1].

*Correspondence to: Babak A. Ardekani, Ph.D., Center for Advanced Brain Imaging, Nathan Kline Institute, 140 Old Orange-burg Rd, Orangeburg, NY 10962, USA. Tel.: +845 398 5490; Fax: +1 845 398 5472; ardekani@nki.rfmh.org..

Authors' disclosures available online (http://www.jalz.com/disclosures/view.php?id=1925).

The CC is readily visualized by magnetic resonance imaging (MRI), particularly its intersection with the mid-sagittal plane. Connection with most of the cortex has made it a target of investigation of brain integrity in Alzheimer's disease (AD). Many modalities, using both structural and diffusion weighted imaging (DWI), have been used to examine the CC for markers of severity and prognosis in AD. Structural studies have included total area, parcellation into multiple regions, and indices of shape. Generally, studies have indicated reduced area primarily in the genu and splenium of the CC. DWI has been used to trace fibers from regions of the CC to cortical areas [2] and to gauge the integrity of those fibers using metrics derived from diffusion tensors such as fractional anisotropy (FA), mean diffusivity (MD), and radial diffusivity (RD) [3].

Reduced FA and increased diffusivities have been observed in the genu and splenium. Di Paola et al. [4] have reviewed many of these studies and found that not all agree with these conclusions. They have suggested that the mechanisms for these changes may be different in the two areas, with myelin breakdown being more important in the genu and Wallerian degeneration in the splenium. This could also affect the staging of the changes, one occurring earlier than the other. Many studies are insensitive to the timing of these changes due to the use of cohorts that are already severely ill, or at a mixture of stages. In addition, the standard deviation of individual measurements is comparable to the differences between groups and the number of individuals in the groups studied have been relatively small (10–20), and these studies have been cross-sectional rather than scanning the same individuals at multiple times. Currently attempts are being made to use many different markers (both structural and diffusion) to describe an individual's condition and prognosis [5].

Atrophy of the brain in AD has been measured by the volume of the whole brain [6–8] and by the volume of structures such as the hippocampus [9–11]. Several studies have indicated that the rate of atrophy of these structures varies with the severity and duration of the disease [6, 7, 12]. The CC mid-sagittal cross-sectional area (CCA) has also been shown to reflect the atrophy of the brain in AD [13, 4 and references therein]. Most of these studies have examined data from a single scan per subject. These studies establish a difference in the CCA and/or its sub-regions (e.g., splenium) between normal controls and groups of AD patients. The study of scan data from a single time-point cannot measure the rate of change of the area, in part due to the difficulty in accurately establishing the time of disease onset. Repeated scans can be used to measure the rate of atrophy. One such result has been reported by Teipel et al. [14] and Hampel et al. [15] with a significantly larger annual atrophy rate of CCA in AD (7.7% ± std. error 6.7%) than that of normal controls (0.9% ± std. error 5.0%). Teipel et al. [14] describe a patient cohort suffering from advanced AD as measured by their Mini-Mental State Exam (MMSE) scores (mean value of 17.4). To our knowledge, there are no existing reports of CC atrophy rates in early AD. Our objective is to study the rate of change of the area and shape of the CC and its sub-regions using longitudinal structural MRI scans of a larger group of subjects at an earlier stage of AD than has been reported before. The recent review by Fred-eriksen and Waldemar [16] also reports the Teipel et al. paper [11] as the only known longitudinal study in which callosal loss rate was measured.

We have used the Open Access Series of Imaging Studies (OASIS) longitudinal database [8] to measure CC atrophy rates for three groups of subjects classified by their clinical dementia ratings (CDR): normal controls (NC, CDR = 0), very mild AD patients (AD-VM, CDR = 0.5) and mild AD patients (AD-M, CDR = 1).

We have previously shown that circularity (CIR), a measure of CC shape, is more sensitive than CCA in differentiating between NC and AD patients [13]. CIR is defined as $4\pi \times CCA/CCP^2$ where CCP denotes the CC perimeter. CIR values range between 0 and 1 (1 being the value for a circle). A factor contributing to the increased sensitivity of CIR is that a non-uniform shrinkage of the CC simultaneously decreases its area and increases its perimeter. In addition, the general atrophic process in the brain that enlarges the lateral ventricles changes the CC shape in a way that would decrease the CIR. In this paper, we measure and compare the rates of change of CCA and CIR, as well as five CC sub-regions. To our knowledge, temporal changes in CC shape have not been studied at any stage of AD. The various acronyms used in this paper are defined in Table 1 for easy reference.

METHODS

Subjects

The OASIS longitudinal database contains 150 right-handed subjects aged 60 to 96. Dementia status was rated by the CDR based solely on clinical methods, without reference to psychometric performance. Details of subject recruitment, assessment, and inclusion/exclusion criteria can be found in the articles by Marcus et al. [8, 17]. We have studied three groups of subjects: normal controls (NC, CDR = 0, $n = 75$), patients with very mild AD (AD-VM, CDR = 0.5, $n = 51$), and patients with mild AD (AD-M, CDR = 1, $n = 21$). We used the first two imaging sessions of each subject in the OASIS database for computing the rates of change of total CC mid-sagittal area (rCCA), its circularity (rCIR), and its five sub-regions (rCC1– rCC5) representing genu, anterior body, mid-body, posterior body, and splenium. The CDR value at the time of the second session was used for grouping the subjects. The demographics of our subjects are listed in Table 2. Delay is the time between the first and second scans.

Image acquisition

The MRI scans are three dimensional sagittal T1-weighted volumes of matrix size 256×256×128 and voxel size 1×1×1.25 mm^3 interpolated to 1 mm^3 isotropic voxels. Each volume is the post registration average of 3 or 4 independently acquired magnetization prepared rapid gradient-echo (MP-RAGE) scans with TR = 9.7 ms, TE = 4.0 ms, TD = 200 ms, TI = 20 ms, and flip angle 10°, using a 1.5 T Vision scanner (Siemens, Erlangen, Germany). Further details of the image acquisition and pre-processing protocols can be found in the articles by Marcus et al. [8, 17].

CC segmentation

Segmentation of the CC on the mid-sagittal section of the brain was accomplished using the Automatic Registration Toolbox (ART) software module ‘yuki’ (http://www.nitrc.org/projects/art) in four automatic steps: 1) Location of the mid-sagittal plane (MSP) [18]; 2)

Location of the anterior and posterior commissures (AC and PC) on the MSP [19]; 3) Standardized reorientation and interpolation of the MSP to 512×512 pixels of size 0.5×0.5 mm^2; and 4) Two-dimensional model-based segmentation of the CC on the standardized MSP [20].

The standardized reorientation in step (3) is based on the detected MSP and the AC and PC landmarks. Using this information, a single 512 × 512 mid-sagittal slice is reconstructed by tri-linear interpolation such that: (a) the slice coincides with the MSP, (b) the image left-to-right axis is the subject's anterior-to-posterior and parallel to the AC-PC line, (c) the image top-to-bottom axis is the subject's superior-to-inferior, and (d) the center of the image field-of-view is the mid-point between the AC and PC.

A more detailed description of the segmentation method can be found in [13].

The final result of CC segmentation is a binary image in which the CC pixels are labeled 1 and non-CC pixels are labeled 0. Each segmentation result was reviewed using a program that overlaid a colored outline of the segmented binary image of the CC on the enlarged mid-sagittal plane image of the brain (obtained in step (3) above). This was performed by a member of the group who was blinded to the diagnostic groups. About 5% of individual segmentations required minor manual corrections.

We were careful to segment the baseline and follow-up scans in exactly the same manor to avoid bias in favor of one time point or the other. The processing of both scans involves a single interpolation operation that created the standardized image described in step (3) above.

Parcellation

The sub-regions of the CC were defined by an automatic procedure following the method proposed by Hampel et al. [15]. The lower tangent of the binary CC image was determined as well as the normal lines to the tangent that touch the anterior and posterior edges of the CC. The mid-point between the two normal lines on the tangent line was used as the center of a set of radii that divided the space of the CC into five equi-angular (36°) sectors. These define the regions CC1–CC5 (genu to splenium). A sample parcellation is shown in Fig. 1. Specifically, the sub-regions are the corpus callosum genu (CC1), anterior body (CC2), mid-body (CC3), posterior body (CC4), and splenium (CC5).

Statistical analysis

We performed ANOVA tests to determine if the three groups (NC, AD-VM, AD-M) differed in age, baseline MMSE, or in the baseline to follow-up delay. Differences in gender distributions were tested by a chi-square test.

To account for the heterogeneity in the delay between baseline and follow-up scans, we utilized a mixed-effects model where delay is considered as a random effect. To be specific, our mixed-effects model is:

$$\Delta = \beta_1 delay + \beta_2 delay \times I_{vm} + \beta_3 delay \times I_m + \in \quad (1)$$

where Δ represents the change over time (follow-up minus baseline) in a parameter (e.g., CIR), delay is a random effect, and I_{vm} and I_m are indicator functions for AD-VM and AD-M groups, respectively. An indicator function takes on the value of 1 if the subject belongs to the corresponding group and a value of 0 otherwise. Note that an intercept term is not included in the model since no change would be expected if there is no delay.

Recognizing that the proportion of female samples to male is not consistent in the three groups (Table 2), we tested the interaction *delay* × *sex* and confirmed that there is no sex effect on Δ with respect to any measures of interest. Therefore, we did not consider a sex effect in subsequent analyses.

The OASIS database also provides a normalized whole brain volume (nWBV) which is used to measure of the overall brain atrophy [8]. To compare the brain atrophy rate with the corpus callosal changes in this cohort, the change in nWBV was also analyzed using the mixed-effects model (1).

Data were analyzed using the procedure '*mixed*' in SAS9.2 for Windows (SAS Institute Inc., Cary, NC). A significance level of 0.05 was used for the tests. Comparisons between means of diagnosis groups were conducted by model-based analyses, i.e., testing the delay by group interactions in model (1). The null hypotheses tested were $\beta_1 = 0$ (zero rate of change in NC), $\beta_1+\beta_2 = 0$ (zero rate of change in AD-VM), $\beta_1+\beta_3 = 0$ (zero rate of change in AD-M), $\beta_2 = 0$ (same rate of change in AD-VM and NC), $\beta_3 = 0$ (same rate of change in AD-M and NC), and finally $\beta_2 = \beta_3$ (same rate of change in AD-VM and AD-M).

RESULTS

Table 3 shows the mean (±std. error) of all variables (CCA, CC1–CC5, CIR and nWBV) measured at the baseline scan. These measurements are consistent with those obtained from the OASIS cross-sectional database [13].

As shown in Table 2, the male/female distributions were significantly different ($p = 0.003$) in the three groups. However, as mentioned before we did not find a *delay* × *sex* interaction in the data and therefore gender was not included as a factor in our mixed-effects model (1). There were no significant age differences ($p = 0.441$) between groups. As expected, the MMSE scores at baseline were significantly different ($p < 0.001$). The average baseline to follow-up delays were also significantly different ($p = 0.006$), being shorter in AD-M patients (1.5 y) than either the NC (2.0 y) or AD-VM (2.1 y) groups. Delay was therefore included as a random effect in our statistical model.

Total CC cross-sectional area (CCA)

Figure 2 shows the rates of change of the total CC cross-sectional area (rCCA). These rates are significantly different from zero for AD-VM ($p < 0.001$) and AD-M ($p < 0.03$) groups. However, the rate is only at trend level significance in the NC group ($p = 0.06$). The 95% confidence interval for the NC being [−3.06, 0.06] (mm^2/y) includes zero. As shown in Table 4, the estimated rates are −1.5, −3.2 and AD-VM, − 4.07 (mm^2/y) for the NC, and AD-M groups, respectively.

Although the rCCA in all three groups of subjects were significantly negative, we did not find them to be statistically different between groups, that is, the null hypotheses $\beta_2 = 0$, $\beta_3 = 0$, and $\beta_2 = \beta_3$ were not rejected. The rCCA atrophy rate as a percentage of the average CCA may be estimated from the data in Tables 3 and 4 to be 0.25%, 0.54%, and 0.69% per year in NC, AD-VM, and AD-M, respectively.

Sub-regional CC areas (CC1–CC5)

Figure 3 shows the rates of change rCC1–rCC5 for the CC sub-regions defined according to Hampel's method [15]. The shrinkage of the genu (rCC1) over time is significant in all three groups (NC: − 0.81 ($p < 0.03$); AD-VM: −1.61 ($p < 0.0003$); AD-M: −2.04 ($p < 0.02$)). The anterior body shrinkage rate (rCC2) was significant in NC ($t = -2.68$ ($p < 0.009$)), at trend level for AD-VM ($t = -1.91$ ($p < 0.06$)), and non-significant in AD-M ($p = 0.473$). Rates for the mid-body (rCC3) and posterior body (rCC4) were not significantly different from zero in any group. Finally, the atrophy rate of splenium (rCC5) was significant in AD-VM ($t = -3.19$ ($p < 0.002$)) and AD-M ($t = -4.41$ ($p < 0.0001$)) groups, but not in NC ($p = 0.337$).

The results also indicated that the rate of atrophy of the splenium (rCC5) was significantly greater in ADM relative to NC ($p < 0.0004$) and in AD-M relative to AD-VM ($p < 0.008$). However, the difference in rates between the AD-VM and NC groups was at trend level significance ($p = 0.08$).

Circularity (CIR)

The rates of change of CC circularity (rCIR) for the three groups of subjects are shown in Fig. 4. These rates were significantly different from zero in all three groups (NC: −0.94 ($p < 0.0002$); AD-VM: −1.78 ($p < 0.0001$); AD-M: −4.13 ($p < 0.0001$)).

Furthermore, the rates of decline in circularity were different between all groups. rCIR was greater (in an absolute sense) in AD-M relative to NC ($p < 0.0001$), in AD-M relative to AD-VM ($p < 0.0004$), and in AD-VM relative to NC ($p < 0.03$).

Whole brain atrophy rate

The whole brain atrophy rates were significantly different from zero in all three groups (NC: −0.00385 ($p < 0.0001$); AD-VM: −0.00498 ($p < 0.0001$); AD-M: −0.01012 ($p < 0.0001$)).

Comparison of the overall brain atrophy rates between the three groups showed that it was faster in AD-M relative to NC ($p < 0.0002$), and faster in AD-M relative to AD-VM ($p < 0.003$). However, the rates of atrophy did not differ between AD-VM and NC groups ($p = 0.264$).

DISCUSSION

Extending our previous observation that circularity provides a sensitive metric of brain integrity in AD [13], we have now demonstrated that this measure is also sensitive to structural brain changes associated with disease progression. Whole brain and splenium atrophy rates were also sensitive to AD progression, however, rCIR was the only measure

that was significantly different between normal controls and patients with very mild AD, which is clearly important for early diagnosis and treatment of AD.

The rate of decline of total CC cross-sectional area, rCCA, while significant in all three groups, was not statistically different between them in our cohort. Our estimated CCA atrophy rates per year (0.25% in NC; 0.54% in AD-VM; 0.69% in AD-M) differ significantly from that of Teipel et al. [14], who reported 7.7% per year. Our mean MMSE values were 26.9 (AD-VM) and 23.5 (AD-M) (Table 2) compared with their 17.4, indicating different populations. We conclude that the atrophy rates increase during the course of the disease.

Fotenos et al. [7] have reported atrophy rates for brain volumes as 0.45% per year for older non-demented individuals and 0.98% per year for those with very mild AD. Chan et al. [6] reported whole brain atrophy rates in the range of 2 to 3% per year for 12 patients with values of MMSE around 23. Again, these values fit together with those of the CC to indicate acceleration of atrophy in the disease.

Using CC size and shape measures to assess the state of the disease in a single individual may be problematic due to the overlapping distributions of values between groups. However mean change values of different groups may be valuable in better understanding the natural history of AD pathology and could play a role in assessing changes in the rate of progression of the disease in response to treatment. The observation that rCIR not only distinguishes AD from normal but also detects differences in progression rates between AD-VM and AD-M also suggests that the irregularity of atrophy may be a valuable starting point for further anatomic studies of atrophy in AD.

We also found the splenium to be the one region of the CC with a significant area rate of change. This is consistent with reports of significant AD-related differences in the area of the splenium from other studies [4, 14]. At this point, it is not clear that this regional effect reflects the typical shape of the splenium or the observations that early in AD, function is reduced in posterior brain regions that include areas interconnected by the CC. DWI tractography has indicated that fibers passing through the splenium connect regions of the temporal, parietal, and occipital lobes [2]. The medial temporal lobe has been cited for changes in the early stages of AD. DWI studies have also indicated a focus on changes in the splenium [3].

The question of whether the CC changes in AD are associated with specific or general changes in mentation cannot be answered with these data.

The size and shape of the CC are highly variable across individuals, depending on age, intracranial volume, gender [21], handedness [22], etc. Using the rate of change of CC size and shape has a self-referential effect that mitigates the added variance due to these factors. However, the remaining variance is still large and class (NC, AD-VM, AD-M) conditional distributions of variables overlap substantially, which makes these variables difficult to use in assessing disease state in single individuals. However, we have demonstrated that some of these variables, particularly the rCIR and rCC5, can be useful as biomarkers to objectively assess the effects of treatments that aim to slow or arrest the progression of AD from very

mild to mild. In addition, although the rCIR and rCC5 may not be sensitive/specific enough for single subject classification, our results indicate that they have sufficient discrimination power to be useful as features in multi-variate, multi-modal pattern analysis methods [23] that may be used to classify single subjects with sufficient accuracy.

ACKNOWLEDGMENTS

This work was supported by R01 DC007658. The Open Access Series of Imaging Studies (OASIS) project was supported under grants: P50 AG05681, P01 AG03991, R01 AG021910, P20 MH071616, and U24 RR021382.

REFERENCES

1. Sidtis JJ, Volpe BT, Holtzman JD, Wilson DH, Gazzaniga MS. Cognitive interaction after staged callosal section: Evidence for transfer of semantic activation. Science. 1981; 212:344–346. [PubMed: 6782673]
2. Hofer S, Frahm J. Topography of the human corpus callosum revisited – Comprehensive fiber tractography using diffusion tensor magnetic resonance imaging. Neuroimage. 2006; 32:989–994. [PubMed: 16854598]
3. Acosta-Cabronero J, Alley S, Williams GB, Pengas G, Nestor PJ. Diffusion tensor metrics as biomarkers in Alzheimer's disease. PLoS One. 2012; 7:e49072. [PubMed: 23145075]
4. Di Paola M, Spalleta G, Caltagirone C. In vivo structural neuroanatomy of corpus callosum in Alzheimer's disease and mild cognitive impairment using different MRI techniques: A review. J Alzheimers Dis. 2010; 20:67–95. [PubMed: 20164572]
5. Alves GS, O'Dwyer L, Jurcoane A, Oertel-Knochel V, Knochel C, Prvulovic D, Sudo F, Alves CE, Valente L, Moreira D, Fuber F, Karakaya T, Pantel J, Engelhardt E, Laks J. Different patterns of white matter degeneration using multiple diffusion indices and volumetric data in mild cognitive impairment and Alzheimer patients. PLoS One. 2012; 7:e52859. [PubMed: 23300797]
6. Chan D, Janssen JC, Whitewell JL, Watt HC, Jenkins R, Frost C, Rossor MN, Fox NC. Changes in rates of cerebral atrophy over time in early-onset Alzheimer's disease: Longitudinal study. Lancet. 2003; 362:1121–1122. [PubMed: 14550701]
7. Fotenos AF, Snyder AZ, Girton LE, Morris JC, Buckner RL. Normative estimates of cross-setional and longitudinal brain volume decline in aging and AD. Neurology. 2005; 64:1032–1039. [PubMed: 15781822]
8. Marcus DS, Fotenos AF, Csernansky JG, Morris JC, Buckner RL. Open access series of imaging studies: Longitudinal MRI data in nondemented and demented older adults. J Cogn Neurosci. 2010; 22:2677–2684. [PubMed: 19929323]
9. Apostolova LG, Dutton RA, Dinov ID, Hayashi KM, Toga AW, Cummings JL, Thompson PM. Conversion of mild cognitive impairment to Alzheimer disease predicted by hippocampal atrophy maps. Arch Neurol. 2007; 63:693–699. [PubMed: 16682538] Erratum in: Arch Neurol (2007) 64, 1360-1361.
10. Jack CR Jr, Peterson RC, Xu Y, O'Brian PC, Smith GE, Ivnik RJ, Boeve BF, Tengalos EG, Kokman E. Rates of hippocampal atrophy correlate with changes in clinical status in aging and AD. Neurology. 2000; 55:484–489. [PubMed: 10953178]
11. Wang L, Swank JS, Glick IE, Gado MH, Miller MI, Morris JC, Csernansky JG. Changes in hippocampal volume and shape across time distinguish dementia of the Alzheimer type from healthy aging. NeuroImage. 2003; 20:667–682. [PubMed: 14568443]
12. Rusinek H, Endo Y, De Sanri S, Frid D, Tsui WH, Segal S, Convit A, de Leon MJ. Atrophy rate in medial temporal lobe during progression of Alzheimer disease. Neurology. 2004; 63:2354–2359. [PubMed: 15623699]
13. Ardekani BA, Bachman AH, Figarsky K, Sidtis JJ. Corpus callosum shape changes in early Alzheimer's disease: An MRI study using the OASIS brain database. Brain Struct Funct. 2013 doi: 10.1007/s00429-013-0503-0.

14. Teipel SJ, Bayer W, Alexander GE, Zebuhr Y, Teichberg D, Kulic L, Shapiro MB, Moller HJ, Rapoport SI, Hampel H. Progression of corpus callosum atrophy in Alzheimer disease. Arch Neurol. 2002; 59:243–248. [PubMed: 11843695]

15. Hampel H, Teipel SJ, Alexander GE, Pogarell O, Rapoport SI, Moller HJ. In vivo imaging of region and cell type specific neocortical neurodegeneration in Alzheimer's disease. J Neural Transm. 2002; 109:837–855. [PubMed: 12111472]

16. Frederiksen KS, Waldemar G. Corpus callosum in aging and neurodegenerative diseases. Neurodegener Dis Manag. 2012; 2:493–502.

17. Marcus DS, Wang TH, Parker J, Csernansky JG, Morris JC, Buckner RL. Open Access Series of Imaging Studies (OASIS): cross-sectional data in young, middle aged, non-demented and demented older adults. J Cogn Neurosci. 2007; 19:1498–1507. [PubMed: 17714011]

18. Ardekani BA, Kershaw J, Braun M, Kanno I. Automatic detection of the mid-sagittal plane in 3-D brain images. IEEE Trans Med Imaging. 1997; 16:947–952. [PubMed: 9533596]

19. Ardekani BA, Bachman AH. Model-based automatic detection of the anterior and posterior commissures on MRI scans. Neuroimage. 2009; 46:677–682. [PubMed: 19264138]

20. Ardekani, BA.; Toshikazu, I.; Bachman, AH.; Szeszko, PR. Proc ISMRM. Melbourne, Australia: 2012. Multi-atlas segmentation with adaptive atlas selection..

21. Ardekani BA, Figarsky K, Sidtis JJ. Sexual dimorphism in the human corpus callosum: An MRI study using the OASIS brain database. Cereb Cortex. 2013; 23:2514–2520. [PubMed: 22891036]

22. Witelson SF. The brain connection: The corpus callosum is larger in left-handers. Science. 1985; 229:665–668. [PubMed: 4023705]

23. Fan Y, Resnick SM, Wu X, Davatzikos C. Structural and functional biomarkers of prodromal Alzheimer's disease: A high-dimensional pattern classification study. Neuroimage. 2008; 41:277–285. [PubMed: 18400519]

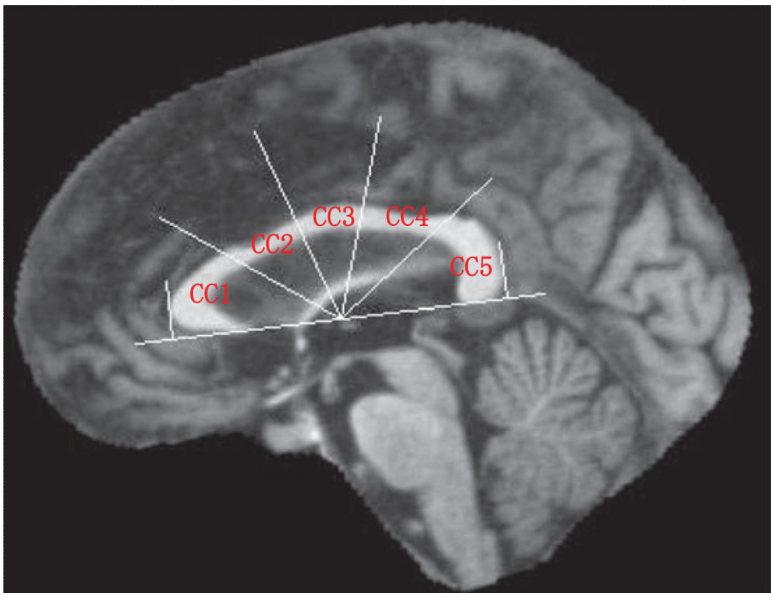

Fig. 1.

Mid-sagittal plane image showing the Hampel's method of parcellation of the corpus callosum.

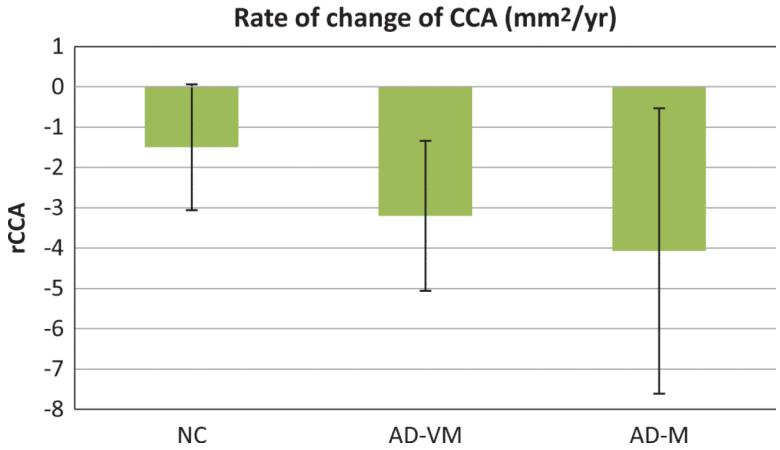

Fig. 2.

Rates of change of the total CC area (rCCA) for normal controls (NC), very mild Alzheimer type dementia patients (ADVM), and mild Alzheimer type dementia patients (AD-M). Patients were classified by Clinical Dementia Ratings of 0.5 and 1. Error bars indicate the 95% confidence interval.

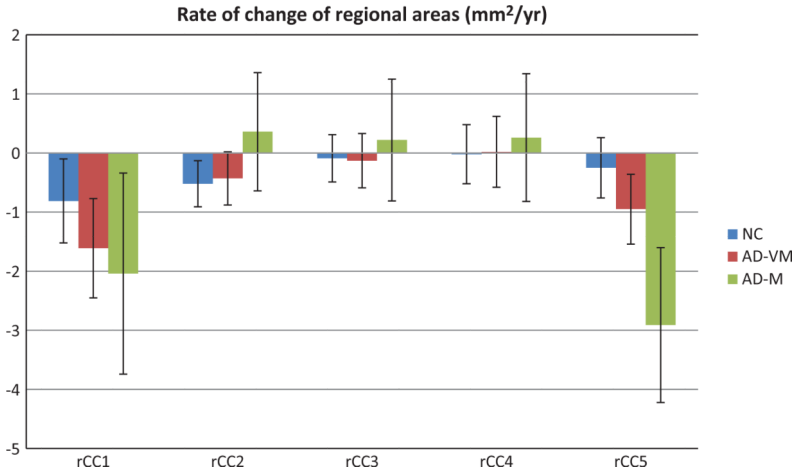

Fig. 3.

Rates of change of areas of the corpus callosum genu (rCC1), anterior body (rCC2), mid-body (rCC3), posterior body (rCC4) and splenium (rCC5), for NC, AD-VM, and AD-M groups. Error bars indicate the 95% confidence interval.

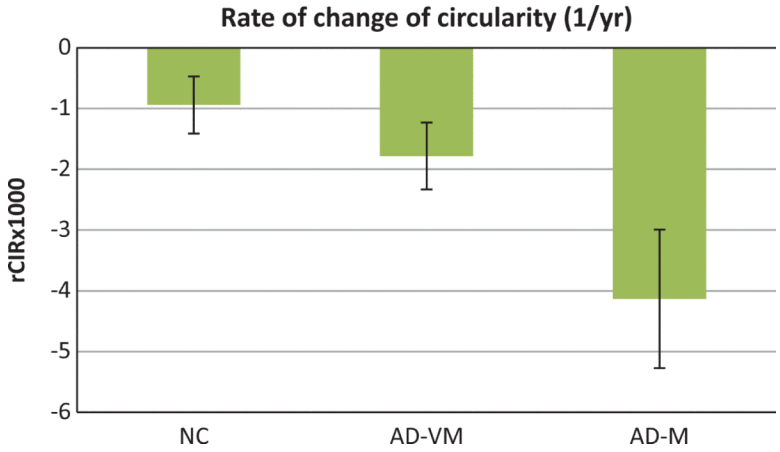

Fig. 4.

Rates of change (1/year) of the corpus callosum circularity (rCIR) for NC, AD-VM and AD-M groups. Error bars indicate the 95% confidence interval.

Table 1

Acronym definitions

CC	corpus callosum
CCA	total cross-sectional area of the CC (mm^2)
rCCA	time rate of change of CCA: $\Delta CCA/\Delta t$ (mm^2/y)
CCP	perimeter of the CC
CIR	CC circularity: $4\pi \times CCA/CCP^2$ (unitless)
rCIR	time rate of change of CIR: $\Delta CIR/\Delta t$ (yr^{-1})
CC*i*	area of CC sub-regions *i* (*i* = 1,2,3,4,5)
rCC*i*	rate of change of CC*i* (mm^2/y)
AD	Alzheimer's disease
OASIS	open access series of imaging studies database
CDR	clinical dementia rating
NC	normal control subjects (CDR = 0)
AD-VM	subjects with very mild AD-type dementia (CDR = 0.5)
AD-M	subjects with mild AD-type dementia (CDR =1)
MRI	magnetic resonance imaging
MP-RAGE	magnetization prepared rapid gradient echo
TR	repetition time
TE	echo time
TD	delay time
TI	inversion time
AC	anterior commissure
PC	posterior commissure
MSP	mid-sagittal plane
DWI	diffusion-weighted imaging
nWBV	normalized whole brain volume

Table 2

Demographic data

	NC	AD-VM	AD-M	p-value
CDR	0	0.5	1	
n (M/F)	75 (21/54)	51 (29/22)	21 (11/10)	0.003
Age (Min/Max)	75.5 (60/93)	75.7 (61/90)	73.4 (64/83)	0.441
MMSE (Min/Max)	29.2 (26/30)	26.9 (17/30)	23.5 (19/30)	<0.001
*Delay (y) (Min/Max)	2.0 (0.5/4.1)	2.1(0.6/4.7)	1.5 (0.7/2.1)	0.006

The *p*-values were obtained from chi-square or ANOVA tests for differences between groups.

*Time between the baseline and follow-up MRI scans.

Table 3

Summary statistics of variables measured at baseline

	NC	AD-VM	AD-M
CCA	608.93 ± 8.71	589.94 ± 11.37	585.92 ± 12.38
CC1	172.74 ± 2.95	167.46 ± 3.87	170.54 ± 4.37
CC2	87.04 ± 1.77	85.39 ± 2.08	82.33 ± 2.36
CC3	79.40 ± 1.64	80.17 ± 2.24	76.24 ± 2.17
CC4	82.69 ± 1.96	81.18 ± 2.51	78.08 ± 3.62
CC5	187.78 ± 2.88	175.74 ± 3.67	178.73 ± 6.64
CIR × 1000	162.06 ± 2.77	156.30 ± 2.53	154.50 ± 5.43
nWBV	0.7457 ± 0.0044	0.7312 ± 0.0048	0.7153 ± 0.0053

Areas in mm^2 ± Standard Error.

Table 4

Rates of change between baseline and follow-up scans

	NC	AD-VM	AD-M
rCCA	–1.50 ± 1.56	–3.20 ± 1.86	–4.07 ± 3.54
rCC1	–0.81 ± 0.71	–1.61 ± 0.84	–2.04 ± 1.70
rCC2	–0.52 ± 0.39	–0.43 ± 0.45	0.36 ± 1.00
rCC3	–0.09 ± 0.40	–0.13 ± 0.46	0.22 ± 1.03
rCC4	–0.02 ± 0.50	0.02 ± 0.60	0.26 ± 1.08
rCC5	–0.25 ± 0.51	–0.95 ± 0.59	–2.91 ± 1.31†‡
rCIR × 1000	–0.94 ± 0.47	–1.78 ± 0.55&	–4.13 ± 1.14§#

Estimates of change per year ± 95% confidence interval. Areal measures are in mm^2 per year. Comparisons:

† rCC5 NC versus AD-M ($p < 0.001$)

‡ rCC5 AD-VM versus AD-M ($p < 0.008$)

& rCIR NC versus AD-VM ($p < 0.024$)

§ rCIR NC versus AD-M ($p < 0.0001$)

rCIR AD-VM versus AD-M ($p < 0.0004$).